International Journal of Biological Macromolecules 227 (2023) 1070–1077

Contents lists available at ScienceDirect

International Journal of Biological Macromolecules

journal homepage: www.elsevier.com/locate/ijbiomac

Magnetically responsive chitosan-pectin films incorporating Fe_3O_4 nanoparticles with enhanced antimicrobial activity

Iratxe Zarandona [a], Daniela M. Correia [b], Joana Moreira [c], Carlos M. Costa [c,d,e], Senentxu Lanceros-Mendez [f,g,*], Pedro Guerrero [a,f,h,**], Koro de la Caba [a,f]

[a] BIOMAT Research Group, University of the Basque Country (UPV/EHU), Escuela de Ingeniería de Gipuzkoa, Plaza de Europa 1, 20018 Donostia-San Sebastián, Spain
[b] Centre of Chemistry, University of Minho, 4710-053 Braga, Portugal
[c] Physics Centre of Minho and Porto Universities (CF-UM-UP), University of Minho, 4710-057 Braga, Portugal
[d] Institute of Science and Innovation for Bio-Sustainability (IB-S), University of Minho, 4710-053 Braga, Portugal
[e] Laboratory of Physics for Materials and Emergent Technologies, LapMET, University of Minho, 4710-057 Braga, Portugal
[f] BCMaterials, Basque Center for Materials, Applications and Nanostructures, UPV/EHU Science Park, 48940 Leioa, Spain
[g] Ikerbasque, Basque Foundation for Science, 48009 Bilbao, Spain
[h] Proteinmat materials SL, Avenida de Tolosa 72, 20018 Donostia-San Sebastián, Spain

ARTICLE INFO

Keywords:
Chitosan-pectin films
Fe_3O_4 nanoparticles
Antimicrobial capacity
Magnetic properties

ABSTRACT

Chitosan-pectin films with iron oxide (Fe_3O_4) magnetic nanoparticles were prepared by solution casting in order to produce biopolymer based magnetically active materials. Infrared (FTIR) spectra indicated physical interactions between the matrix and nanoparticles, corroborated by differential scanning calorimetry (DSC) results. In addition, thermal characterization suggested that the interactions between chitosan, pectin and the nanoparticles resulted in a less compact structure, influencing the film mechanical properties. Regarding vibrating-sample magnetometry (VSM) and electrical analysis, chitosan-pectin films with Fe_3O_4 nanoparticles showed ferrimagnetic behavior, with an increase of the dielectric constant as the nanoparticle concentration increased. Furthermore, films displayed enhanced antimicrobial activity against *Escherichia coli* (Gram-negative) and *Staphylococcus epidermidis* (Gram-positive) bacteria. Therefore, chitosan-pectin films with Fe_3O_4 magnetic nanoparticles provide promising results for active and intelligent food packaging applications.

1. Introduction

Food packaging plays an essential role in the food supply chain, guaranteeing food quality and safety from external factors, such as microorganisms, temperature, odors and light exposure, during food transport and storage, and supporting the prevention of food waste [1]. In this regard, packaging technologies are in continuous evolution seeking to improve the quality and freshness of food and prolonging its shelf life [2]. Additionally, with the goal of attenuate environmental issues and to implement circular economy models, sustainable materials are gaining relevance as potential candidates for food packaging [3]. Particularly, biopolymers could be a sustainable alternative for packaging materials due to their biodegradable character and non-toxicity [4–6]. Among the different biopolymers, and due to their specific properties, chitosan and pectin could be suitable materials for intelligent packaging films, since both polysaccharides are pH dependent. Under low pH conditions, positively charged chitosan and negatively charged pectin bind *via* ionic interactions forming a polyelectrolyte complex, resulting in the enhancement of the mechanical properties and hydrophilicity over chitosan and pectin matrices separately [7,8]. Few works have been reported on the use of chitosan-pectin matrix for food packaging. Among them, [9] prepared chitosan-pectin films with anthocyanin as a pH indicator device for intelligent food packaging, and [10] added *Streptomyces coelicolor*, which improved CO_2 barrier properties to the film.

Regarding intelligent packaging, the aim is to monitors physical, chemical or biological status of food items by detectors and sensors, from the beginning of the food supply chain until it reaches the

* Correspondence to: S. Lanceros-Mendez, BCMaterials, Basque Center for Materials, Applications and Nanostructures, UPV/EHU Science Park, 48940 Leioa, Spain.
** Correspondence to: P. Guerrero, BIOMAT Research Group, University of the Basque Country (UPV/EHU), Escuela de Ingeniería de Gipuzkoa, Plaza de Europa 1, 20018 Donostia-San Sebastián, Spain.
E-mail addresses: senentxu.lanceros@bcmaterials.net (S. Lanceros-Mendez), pedromanuel.guerrero@ehu.es (P. Guerrero).

https://doi.org/10.1016/j.ijbiomac.2022.11.286
Received 13 July 2022; Received in revised form 21 November 2022; Accepted 28 November 2022
Available online 1 December 2022

Table 1
Composition of chitosan-pectin films with different contents of Fe_3O_4 nanoparticles.

System designation	Chitosan concentration (wt%)	Pectin concentration (wt %)	NP concentration (wt%)
Control	50.00	50.00	0
0.1NP	49.95	49.95	0.1
0.5NP	49.75	49.75	0.5
1NP	49.50	49.50	1
5NP	47.50	47.50	5
10NP	45.00	45.00	10

consumer, providing information about the food quality and internal environment conditions of the package [11,12]. Thus, intelligent packaging can provide information of the *in situ* conditions of the food quality and freshness, leading to a loss of dependency on food expiry dates. In this regard, nanoparticles of metal oxides have a great potential for applications in food industry because of their antibacterial capacity, non-toxicity, oxygen and ethylene scavenging capability, and thermal stability properties [13]. Indeed, metal oxides show sensing properties by the mechanism of adsorption and desorption with different gaseous compounds on the surface of the material, leading to changes in the electrical conductance [14]. In this regard, Fe_3O_4 nanoparticles (NP) have been applied in a variety of including biomedicine, cosmetics and food preservation, due to their antimicrobial activity, magnetic response, biocompatibility and non-toxic properties [15,16]. For food applications, Fe_3O_4 NPs have been used as sensors for detecting different compounds, such as heavy metals [17], caffeic acid (Department of Food Science and Technology, Ayatollah Amoli Branch, Islamic Azad University, Amol 46311-39631, Mazandaran, Iran; & Abdi, [18]), or foodborne spoilage bacteria [19].

In this context, the aim of the present work was to prepare chitosan-pectin films with Fe_3O_4 nanoparticles by solution casting, in order to assess the effect of Fe_3O_4 NPs concentrations on the chitosan-pectin matrix, physicochemical, thermal, structural, magnetic, electric and antimicrobial properties.

2. Materials and methods

2.1. Materials

Chitosan with a molecular weight of 375 kDa and a deacetylation degree ≥75 % was supplied by Sigma-Aldrich, Spain. High methoxylated pectin, with a molecular weight of 472 kDa and an esterification degree of 58 %, was kindly supplied by CEAMSA, Spain. Iron oxide (Fe_3O_4) powder, with particle size of 50–100 nm and a purification degree of 97 %, was supplied by Nanostructured & Amorphous Materials, Inc., USA. Acetic acid solution (1 N), used as solvent, was supplied by Panreac, Spain.

2.2. Film preparation

Chitosan-pectin films with Fe_3O_4 nanoparticles were processed by solution casting. The polymers were dissolved separately. On the one hand, the required amount of chitosan was dissolved in 1 wt% acetic acid solution by stirring for 30 min. On the other hand, Fe_3O_4 nanoparticles were dispersed in a 0.1 wt% aqueous solution of Triton 100-X by sonication for 3 h. Then, the required amount of pectin was added to the NP aqueous solution and stirred at 67 °C. Both solutions were mixed at 8000 rpm for 10 min (Ultraturrax UT25, IKA, Germany), and air bobbles were removed by vacuum. The mixture was placed in a petri dish and left to dry at room temperature. Mixture compositions incorporating Fe_3O_4 NP concentrations between 0.1 and 10 wt% are shown in Table 1.

2.3. Film characterization

2.3.1. Fourier transform infrared (FTIR) spectroscopy

An Alpha II spectrometer (Bruker, Madrid, Spain), with a Platinum ATR accessory, was used to collect FTIR spectra of chitosan-pectin films with Fe_3O_4 nanoparticles. A total of 32 scans were performed with a resolution of 4 cm^{-1} in the wavelength between 4000 and 800 cm^{-1}.

2.3.2. Thermo-gravimetric analysis (TGA)

A Mettler Toledo TGA/SDTA 851 thermo-balance was used to measure the thermal stability of the samples. Dynamic scans from 25 to 900 °C were carried out at a constant rate of 10 °C/min under nitrogen atmosphere to avoid thermo-oxidative reactions.

2.3.3. Differential scanning calorimetry (DSC)

A Mettler Toledo DSC 822 was used to perform differential scanning calorimetry. Samples of around 3 mg were heated from −50 °C to 300 °C at a heating rate of 10 °C/min under nitrogen atmosphere to avoid oxidative reactions.

2.3.4. Scanning electron microscopy (SEM)

Morphology was examined by using a Hitachi S-4800 scanning electron microscope at an accelerating voltage of 15 kV. Before analysis, fractured surfaces were coated with a gold layer by sputtering with a Polaron SC502 apparatus.

Additionally, scanning electron microscopy/energy-dispersive X-ray spectroscopy (SEM/EDX) was used to analyze the particle distribution within the samples with a Hitachi TM3000 Tabletop Microscope.

2.3.5. Mechanical properties

Mechanical properties were measured with an Instron 5967 electromechanical testing system (Instron, Spain). According to ASTM D638-14 [20], tests were carried out with a load cell of 500 N and a crosshead rate of 1 mm/min. Films were cut into bone shaped samples of 4.75 mm × 22.25 mm. Five samples were measured for each system. Tensile strength (TS), elongation at break (EAB) and elastic modulus (E) were evaluated from the measurements.

2.3.6. Vibrating-sample magnetometry (VSM)

The magnetic properties of the films were analyzed with a Micro-Sense EZ7 VSM from −1.8 to 1.8 T at room temperature. The hysteresis loops of the samples were measured and remanence (M_r), magnetization saturation (M_s) and coercive field (H_c) parameters were obtained.

2.3.7. Electrical characterization

For the electric measurements, circular gold electrodes of 5 mm diameter were deposited by magnetron sputtering with a Polaron Coater SC502 onto both sides of each sample. The electrical conductivity of the films was measured through a Keithley 487 picoammeter/voltage source with a ± 10 *V* voltage, and the volume conductivity of the films (σ) was calculated by:

$$\sigma = \frac{d}{R.A} \quad (1)$$

where *R* is the resistance of the film obtained from the slope of the *I–V* curves, *d* is thickness, and *A* is the electrode area.

Dielectric measurements were performed using a Quadtech 1920 LCR precision meter. The capacitance (C) and the dielectric losses (tan δ) were obtained at room temperature in the frequency range from 20 Hz to 1 MHz with an applied voltage of 0.5 V.

The real (ε') part of the dielectric function was calculated as:

$$\varepsilon' = \frac{C \cdot d}{\varepsilon_0 \cdot A} \quad (2)$$

where C is the individual sample capacity, ε_0 is the permittivity of

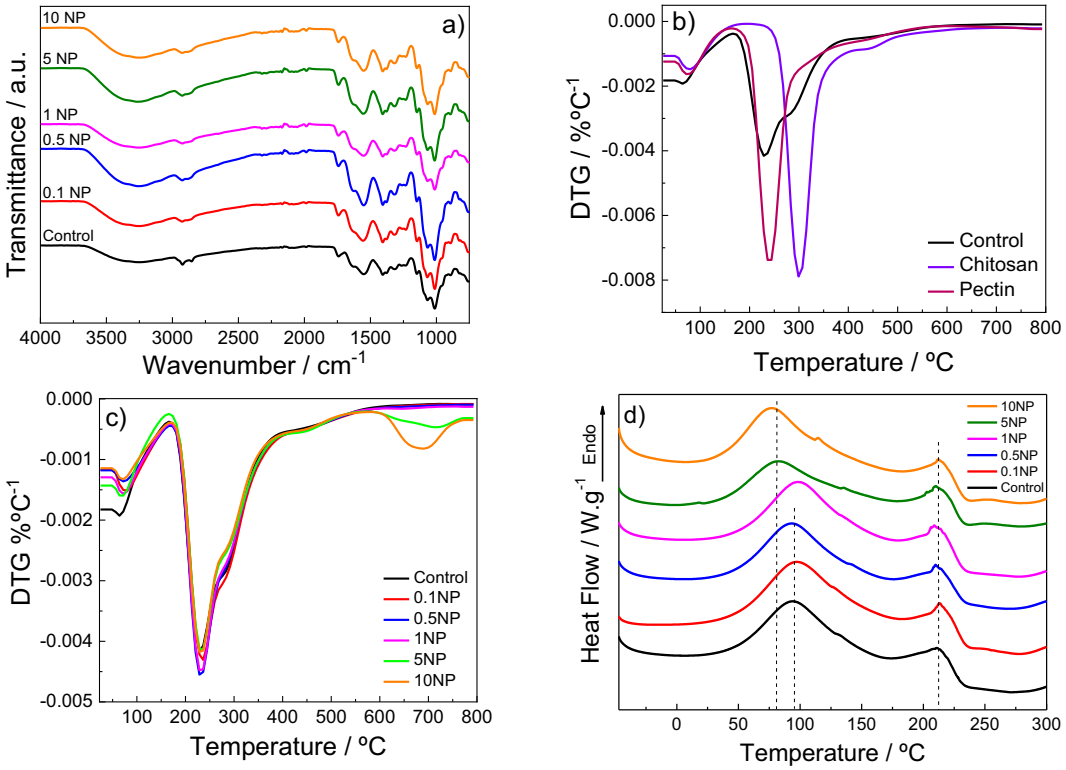

Fig. 1. a) FTIR spectra of chitosan-pectin films, b) DTG of neat chitosan, neat pectin and control film, c) DTG of chitosan-pectin films and d) DSC of chitosan-pectin films.

vacuum (8.85×10^{-12} F·m^{-1}), A is the electrode area and d is the film thickness.

The real part of the conductivity of the dielectric material can be calculated from the dielectric measurements as follows:

$$\sigma'(\omega) = \varepsilon_0 \omega \varepsilon''(\omega) \tag{3}$$

where ε_0 is the permittivity of free space, $\omega = 2\pi f$ is the angular frequency and $\varepsilon''(\omega) = \varepsilon' \tan\delta$ is the frequency dependent imaginary part of the dielectric permittivity.

2.3.8. Antimicrobial analysis

To determine the inhibition capacity of films, two food pathogens were tested: a Gram negative *E. coli* K12 and a Gram-positive *Staphylococcus epidermidis* NCTC 11,047 purchased from American Type Culture Collection (LGC Standards S.L.U.) The bacterial pre-inoculum was prepared by using a single colony from the corresponding stock and resuspended in nutrient broth (NB). After incubating overnight at 37 °C and 200 rpm, the pre-inoculum was centrifuged (5000 rpm) and the pellet was resuspended in 0.9 % solution of NaCl at pH 6.5. The optical density, OD, of *E. coli* and *S. epidermidis* was measured at 600 nm and adjusted to 0.28 ± 0.01 and 0.36 ± 0.01 for *E. coli* and *S. epidermidis*, respectively.

Samples were cut in circular pieces of 10 mm diameter, placed into falcons, and sterilized with ultraviolet light for 30 min on each side. Then, 2 mL of the final bacterial suspension was added and came into contact with the films for 2 h at 37 °C and 200 rpm. Falcons without any material were used as controls for bacterial growth.

The viability of bacterial cells in suspension after contacting the material was evaluated using colony-forming units (CFUs) assay. Ten-fold serial dilutions of the bacterial cultures of the falcons were carried out in 0.9 % NaCl aqueous solution. A volume of 10 μL was placed on spread plates of NB and colony-forming units per milliliter (CFU · mL^{-1}) count was carried out after incubating the plates at 37 °C for 24 h. Antimicrobial activity was determined by comparing viable bacteria of each system with that incubated without any film. The bacterial growth inhibition was calculated based on the following equation:

$$\text{Bacterial growth inhibition } (\%) = 100 - \left(\frac{CFU\ sample}{CFU\ control}\right) \times 100\% \tag{4}$$

2.4. Statistical analysis

With the purpose of determining the significant differences between measurements, analysis of variance (ANOVA) was carried out by means of SPSS software (SPSS Statictic 25.0). Tukey's multiple range test was used for multiple comparisons among different systems with a statistical significance at the $p < 0.05$ level.

3. Results and discussion

3.1. FTIR analysis and thermal characterization

In order to evaluate the interactions among the components of the films, FTIR analysis was carried out and the spectra are shown in Fig. 1a). The characteristic bands of chitosan and pectin were observed in control films: the band at 3247 cm^{-1}, associated to O—H bonds in both polymers and to N—H bonds in chitosan; the bands between 2925 and 2850 cm^{-1}, attributed to C—H stretching vibrations; the band at 1742 cm^{-1}, associated to C═O in the ester bonds of pectin; the band at 1633 cm^{-1}, assigned to the stretching of C═O bond in chitosan and to the asymmetric stretching of COO^- in pectin; and the band between 1150 and 890 cm^{-1}, attributed to the C-O-C of the saccharide ring of chitosan and pectin. As shown in a previous study, the bands related to C═O stretching of chitosan and to the ester bond of pectin showed displacements towards lower wavenumbers, indicating that the interactions between chitosan and pectin were physical [21].

Additionally, some bands displacements were observed when Fe_3O_4 nanoparticles were added into the chitosan-pectin system. In particular,

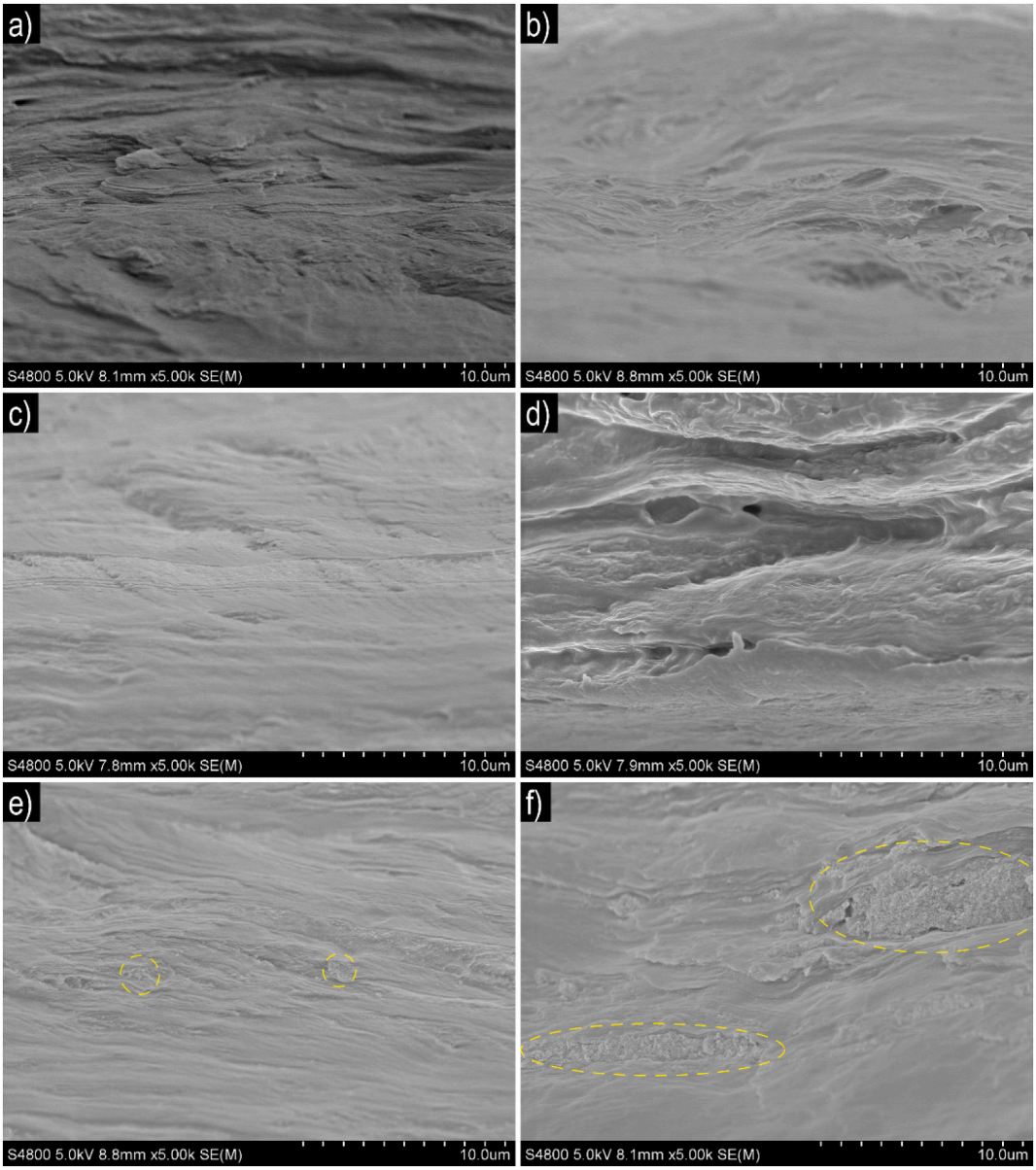

Fig. 2. SEM images of chitosan-pectin film cross-section: a) control, b) 0.1NP, c) 0.5NP, d) 1NP, e) 5NP, and f) 10NP. Yellow dashed circles indicate nanoparticle aggregations.

O—H and N—H vibration bands shifted to higher wavenumbers, from 3247 cm^{-1} for control films up to 3263 cm^{-1} for 10NP, as the nanoparticle concentration increased. Moreover, the band associated to C—H stretching vibrations at 2853 cm^{-1} shifted to higher wavenumbers, becoming a shoulder of the band at 2923 cm^{-1}. All these band displacements indicated that Fe_3O_4 nanoparticles interacted physically with chitosan-pectin matrix.

TGA and DSC analyses were carried out in order to determine the thermal stability of the material. Concerning TGA, derivative thermogravimetric curves are presented in Fig. 1b and c. Regarding neat chitosan and pectin samples (Fig. 1b), thermal degradation was observed at 300 °C and 240 °C, respectively. For control films, 4 inflection points were presented. The first one was observed around 68 °C, related to the water evaporation due to moisture. The second inflection point, around 230 °C, was the greatest one and it was related to the thermal degradation of chitosan and pectin polymers. It should be noted that the thermal degradation of chitosan-pectin film happened at lower temperature than that of pure pectin and pure chitosan (Fig. 1b). This event could indicate that the ionic bonding between chitosan and pectin led to structure changes in the material [9]. The third inflection peak was a shoulder at 283 °C, related to the chitosan that was not bonded to pectin. Finally, a slight inflection point was observed at 447 °C, related to the decomposition of by-products. The addition of Fe_3O_4 nanoparticles (Fig. 1c) caused the presence of a new inflection peak around 680 °C, which became more intense as the concentration of NP increased and can be attributed to the transition from Fe_3O_4 to FeO [22].

The endothermic peaks for the DSC thermogram of chitosan-pectin systems with Fe_3O_4 NP are shown in Fig. 1d. Two endothermic peaks were observed for control films: the first, at 94 °C, was attributed to the film moisture; the second, at 211 °C, was related to the entrapped water linked by hydrogen bonding with the polar groups of the biopolymers [23]. Regarding the films with nanoparticles, the same endothermic peaks were observed as for the control sample, although for the samples with higher concentration of nanoparticles, 5NP and 10NP, the peak at 94 °C for the control sample was shifted to lower temperatures, 82 °C and 76 °C, respectively. This displacement indicated that there were interactions between the matrix and the NP, as observed by FTIR. In addition, the shift to lower temperatures would indicate that the

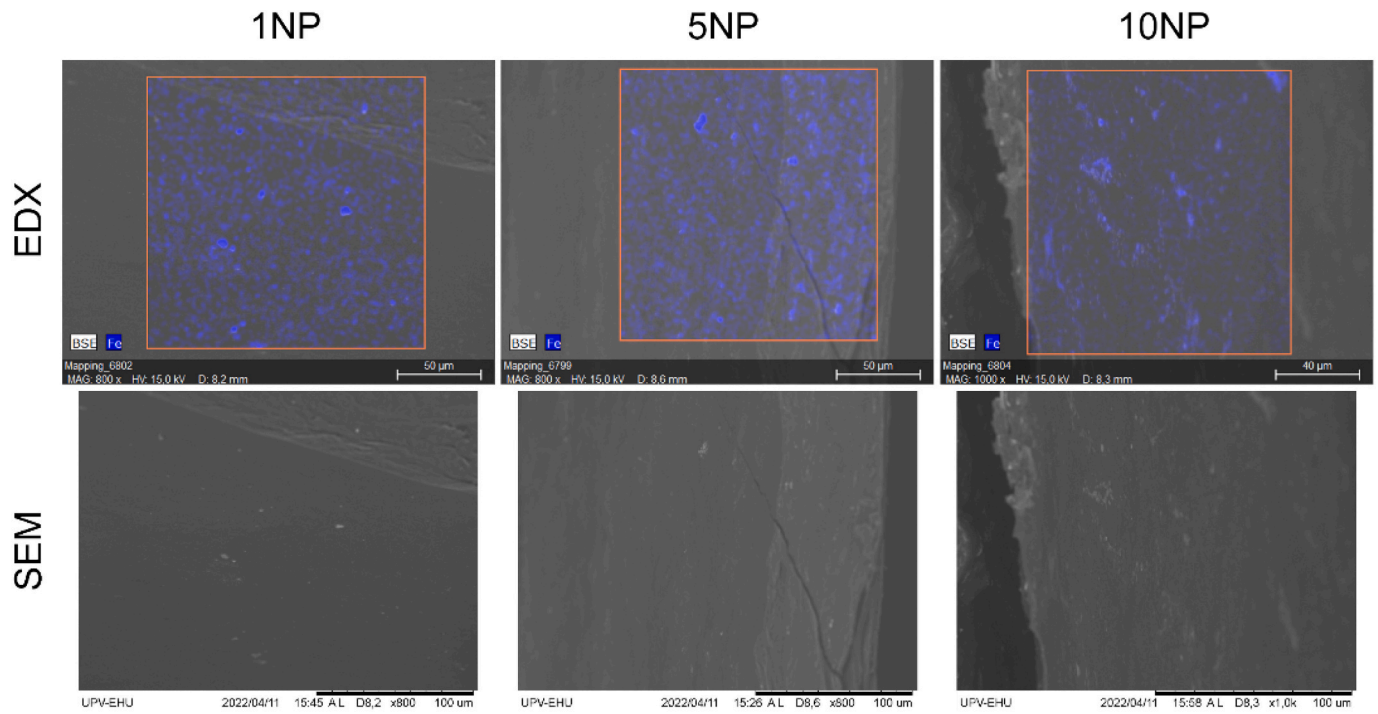

Fig. 3. SEM/EDX images of the surface of chitosan-pectin films with 1 % Fe_3O_4 (1NP), 5 % Fe_3O_4 (5NP) and 10 % Fe_3O_4 (10NP).

Table 2
Tensile strength (TS), elongation at break (EAB) and elastic modulus (E) of chitosan-pectin films without Fe_3O_4 nanoparticles (Control) and with different contents of Fe_3O_4 nanoparticles.

Films	TS (MPa)	EAB (%)	E (MPa)
Control	47.0 ± 1.1^a	6.0 ± 0.5^a	2395 ± 52^a
0.1NP	43.7 ± 1.2^b	5.9 ± 0.2^a	2397 ± 18^a
0.5NP	43.9 ± 1.2^b	6.0 ± 0.6^a	2443 ± 27^a
1NP	44.0 ± 0.5^b	6.3 ± 0.8^a	2417 ± 40^a
5NP	40.7 ± 0.8^c	7.0 ± 0.5^a	2076 ± 58^b
10NP	40.1 ± 1.0^c	7.0 ± 0.7^a	2053 ± 46^b

a-c: Two means followed by the same letter in the same column are not significantly ($p > 0.05$) different according to the Tukey's multiple range test.

structure formed was less compact and, therefore, would require less energy to release the moisture.

3.2. Structure and mechanical properties

The morphology of the films was analyzed by SEM and the cross-section images of the samples are shown in Fig. 2. Control films presented a homogeneous structure, indicating the compatibility between chitosan and pectin. When Fe_3O_4 nanoparticles were added at low concentrations, the structure of the films remained homogeneous but, as NP concentration increased, especially for 5NP and 10NP samples, nanoparticle aggregations were observed. In particular, the nanoparticle clustering in 10NP films was bigger than in 5NP films. These results explain the temperature decrease observed by DSC analysis, since the nanoparticle aggregations led to a less compact polymer structure.

The dispersion of iron on 1NP, 5NP and 10NP films surface was analyzed by SEM/EDX. As can be observed in Fig. 3, the Fe signal in blue showed that the nanoparticles were homogeneously dispersed through the surface of the films, though larger NP aggregates are shown for the samples with larger filler contents.

Tensile strength (TS), elongation at break (EAB), and elastic modulus (E) of the films, shown in Table 2, were measured in order to assess the influence of the magnetic nanoparticles on the chitosan-pectin matrix. Regarding to control films, high values of TS were obtained, due to the strong intermolecular bonds between chitosan and pectin, which derived into a compact structure. These values are higher than those

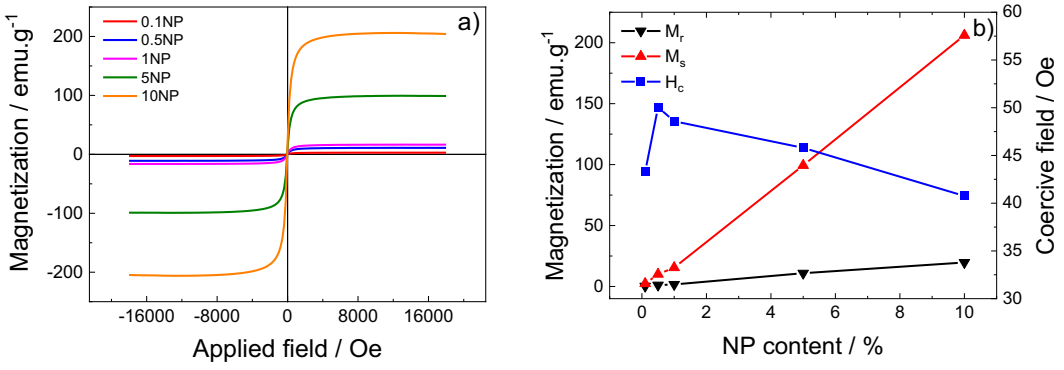

Fig. 4. a) Hysteresis loops and b) magnetic properties (Mr, remanence; magnetization saturation, Ms.; and Hc, coercive field) of chitosan-pectin films with different contents of Fe_3O_4 nanoparticles.

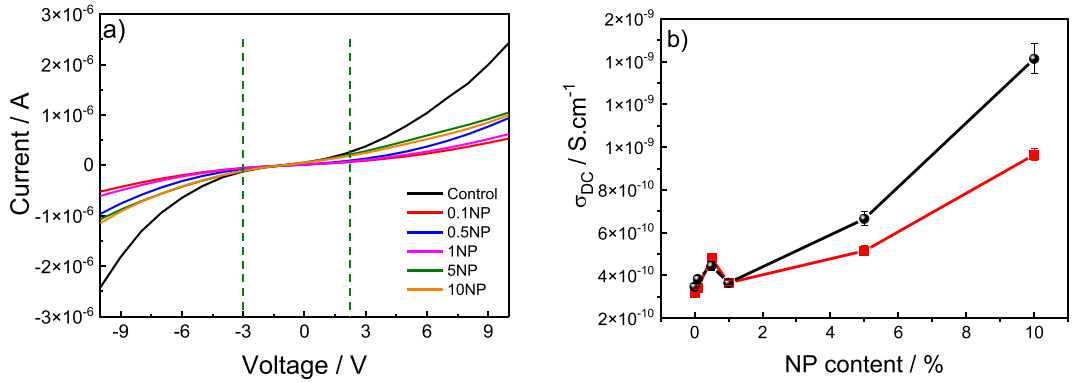

Fig. 5. a) Current-voltage (*I-V*) curves and b) electrical conductivity value of films as a function of Fe_3O_4 content in the 1st regime (black) and in the 2nd regime (red).

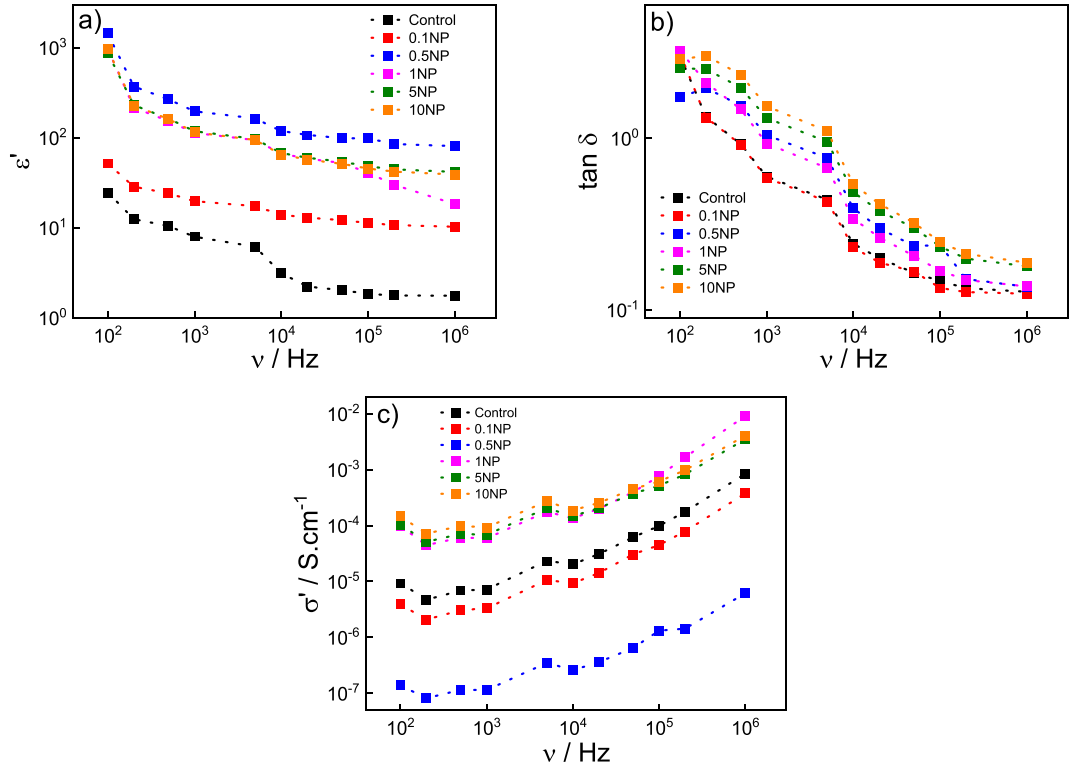

Fig. 6. a) Real part of dielectric constant (ε'), b) dielectric losses (tan δ), and c) a.c. conductivity (σ') of chitosan-pectin films with different contents of Fe_3O_4 nanoparticles.

found by other authors for chitosan-pectin films [24]. When the nanoparticles were added, no significant differences ($p > 0.05$) were observed in EAB results. However, TS values decreased as the nanoparticles concentration increased, as well as E values for 5NP and 10NP, indicating that the NP acts as defective sites for mechanical properties, in particular for concentrations >5 %. These results indicate that Fe_3O_4 nanoparticles affected the structure of the polymeric matrix, as observed in SEM images, hindering the interactions between chitosan and pectin chains [25].

3.3. Magnetic properties

Regarding magnetic properties, VSM analysis was carried out to obtain the hysteresis loops and calculate the remanence, the magnetization saturation, and the coercive field (Fig. 4). The systems exhibited a ferrimagnetic behavior, since the values of remanence and coercive field were unequal to zero [26]. As observed in Fig. 4b, the magnetic behavior of the systems was dependent of the nanoparticle concentration. As the nanoparticle concentration increased, M_r values increased, from 0.23 emu/g (0.1NP) to 19.70 emu/g (10NP), as well as M_s values from 2.38 emu/g (0.1NP) to 206.11 emu/g (10NP). However, coercive field increased as nanoparticle concentration increased up to 0.5 % (50 Oe) but started to decrease until 41 Oe (10NP) as nanoparticle concentration increased. The coercive field is dependent on the nanoparticle size: if the size increases, the coercivity increases until a critical particle size is reached, after which the coercivity decreases. Nevertheless, since the size of the nanoparticles in this study are the same for all samples, results may be related to the agglomeration of the nanoparticles, as described in previous works [27].

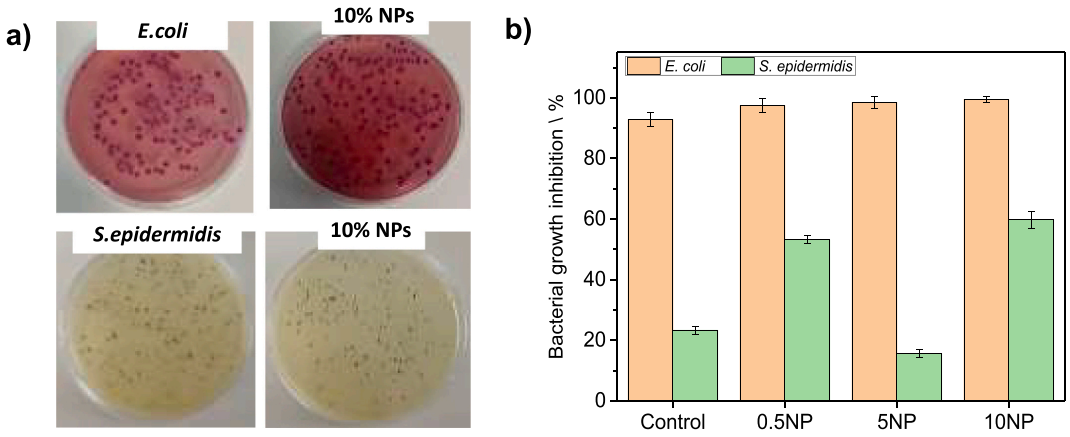

Fig. 7. a) Photographs of the antimicrobial activity against *E. coli* and *S. epidermis* for chitosan-pectin films with 10 wt% of Fe_3O_4 nanoparticles, and b) inhibition capacity of chitosan-pectin films, without Fe_3O_4 nanoparticles (Control) and with different contents of Fe_3O_4 nanoparticles, against *E. coli* and *S. epidermidis* strains in solution after 2 h in contact with material. The results are the average of 3 independent assays.

3.4. Electric characterization

Electrical conductivity of the films with Fe_3O_4 nanoparticles was evaluated by performing I-*V* curves (Fig. 5a). It can be observed that the I-V curves depend on the Fe_3O_4 content and does not present the straight-line dependence characteristics of Ohm's law. Instead, two regimes are observed at low (−10 V to −3 V) and high applied voltages (2 V to 10 V). These regimes are related to the water linked by hydrogen bonding of the polar groups and the movement of free ions by the application of the electric field. As can be observed in Fig. 5b, the electrical conductivity increases strongly as a function of Fe_3O_4 content for both regimes. The electrical conductivity of control films and 10NP films was 3.2×10^{-10} S·cm^{-1} and 9.6×10^{-10} S·cm^{-1}, respectively in the 2nd regime. This behavior is due to the fact that the addition of Fe_3O_4 nanoparticles increases the charge carriers and the conduction is assigned to the electron hopping.

Additionally, the dielectric analysis was evaluated and results are shown in Fig. 6. The dielectric constant (Fig. 6a) and tan δ (Fig. 6b) depend on the frequency due to dipole relaxation. Regardless of frequency range, the dielectric constant and tan δ increases as a function of NP concentration due to polarization contributions derived from the addition of nanoparticles, mainly dominated by interfacial and spatial charge polarization [28]. Concerning a.c. conductivity (Fig. 6c), values increased with frequency, indicating the local contribution to the electrical conductivity. Regardless of frequency range, the addition of Fe_3O_4 nanoparticles increased the a.c. conductivity due to the charge carrier hopping [29].

3.5. Antimicrobial capacity

All films showed antimicrobial activity against *E. coli* and *S. epidermis* as can be seen in the representative photographs presented in Fig. 7a, although different response was observed for both bacteria (Fig. 7b). In the case of *S. epidermidis*, 10 NP films reached 43 % of inhibition, while 98 % was reached for *E. coli*. The antimicrobial capacity of the films was driven by both chitosan and magnetic nanoparticles. The antimicrobial mechanism of chitosan was caused by the positive charge of the amino group of chitosan, which interacted with the negative charges of cell membranes, affecting the loss of protein and other intracellular components [30]. On the other hand, the antimicrobial effect of iron nanoparticles was related to the capacity of the nanoparticles to interact with the cell membrane and to penetrate inside the cells, causing membrane damage and inactivation of the bacteria [31]. Therefore, chitosan-pectin films with Fe_3O_4 nanoparticles showed increased antibacterial activity due to the cooperative action of chitosan and Fe_3O_4 nanoparticles.

It is worth noting that Fe_3O_4 nanoparticles improved antimicrobial capacity when compared to control films. Additionally, it should be noted the difference in the inhibitory capacity of the films with respect to the two bacteria under study. This difference might be due to the different cell walls of Gram-positive and Gram-negative bacteria. The cell wall of Gram-positive bacteria consists of an outer thick layer of peptidoglycan that acts as a layer of resistance against most inhibitory molecules, whereas the cell wall of Gram-negative bacteria has a thinner peptidoglycan layer [32].

4. Conclusions

The preparation of chitosan-pectin films with Fe_3O_4 magnetic nanoparticles by solution casting led to homogeneous films. FTIR results indicated that the physical interactions between chitosan and pectin were not affected by the addition of the nanoparticles. However, the mechanical properties were influenced by Fe_3O_4 nanoparticles, due to the aggregation of the nanoparticles, as shown by SEM. The incorporation of nanoparticles also influenced the electrical, magnetic and antimicrobial properties. As the nanoparticle concentration increased, the dielectric constant, the remanence and the magnetization saturation increased. For the antimicrobial properties, the addition of the nanoparticles increased the antimicrobial capacity of the films for pathogenic *Escherichia coli* (Gram-negative) and *Straphylococcus epidermidis* (Gram-positive) bacteria. Therefore, Fe_3O_4 nanoparticles incorporated into chitosan-pectin films forming solutions could extend food shelf-life, besides functioning as a potential sensor for food packaging due to their electric and magnetic properties.

CRediT authorship contribution statement

Iratxe Zarandona: Data curation, Formal analysis, Investigation, Writing – original draft. **Daniela M. Correia:** Data curation, Formal analysis, Investigation, Methodology, Writing – original draft. **Joana Moreira:** Data curation, Formal analysis, Investigation, Methodology, Writing – original draft. **Carlos M. Costa:** Conceptualization, Investigation, Methodology, Resources, Funding acquisition, Supervision, Validation, Writing – review & editing. **Senentxu Lanceros-Mendez:** Conceptualization, Investigation, Resources, Funding acquisition, Supervision, Validation, Writing – review & editing. **Pedro Guerrero:** Conceptualization, Investigation, Methodology, Supervision, Validation, Writing – review & editing. **Koro de la Caba:** Conceptualization, Investigation, Resources, Funding acquisition, Supervision, Validation, Writing – review & editing.

Declaration of competing interest

The authors declare that they have no known competing financial interests or personal relationships that could have appeared to influence the work reported in this paper.

Acknowledgments

Grant PID2021-124294OB-C22 funded by MCI/AEI10.13039/501100011033 and by "ERDF A way of making Europe". Biomat group thanks the Basque Government for funding (IT1658-22) and I.Z. thanks the Basque Government for her fellowship (22-2018-00078). This work was also supported by the Portuguese Foundation for Science and Technology (FCT) under strategic funding UIDB/04650/2020, UID/FIS/04650/2021, project PTDC/FIS-MAC/28157/2017, and Investigator FCT Contracts 2020.02915.CEECIND (D.M.C) and 2020.04028.CEECIND (C.M.C.) funded by national funds through FCT and by the ERDF through the COMPETE2020-Programa Operacional Competitividade e Internacionalização (POCI). Thanks are also due to the Advanced Research Facilities (SGIker) from the UPV/EHU.

References

[1] A.C. Mendes, G.A. Pedersen, Perspectives on sustainable food packaging:– is bio-based plastics a solution? Trends Food Sci. Technol. 112 (2021) 839–846, https://doi.org/10.1016/j.tifs.2021.03.049.
[2] L.R. Magnaghi, C. Zanoni, G. Alberti, P. Quadrelli, R. Biesuz, Towards intelligent packaging: BCP-EVOH@ optode for milk freshness measurement, Talanta 241 (2022), 123230, https://doi.org/10.1016/j.talanta.2022.123230.
[3] S. Quattrosoldi, G. Guidotti, M. Soccio, V. Siracusa, N. Lotti, Bio-based and one-day compostable poly(diethylene 2,5-furanoate) for sustainable flexible food packaging: effect of ether-oxygen atom insertion on the final properties, Chemosphere 291 (2022), 132996, https://doi.org/10.1016/j.chemosphere.2021.132996.
[4] O.M. Atta, S. Manan, A. Shahzad, M. Ul-Islam, M.W. Ullah, G. Yang, Biobased materials for active food packaging: a review, Food Hydrocoll. 125 (2022), 107419, https://doi.org/10.1016/j.foodhyd.2021.107419.
[5] S. LakshmiBalasubramaniam, C. Howell, M. Tajvidi, D. Skonberg, Characterization of novel cellulose nanofibril and phenolic acid-based active and hydrophobic packaging films, Food Chem. 374 (2022), 131773, https://doi.org/10.1016/j.foodchem.2021.131773.
[6] W. Zhang, J.-W. Rhim, Recent progress in konjac glucomannan-based active food packaging films and property enhancement strategies, Food Hydrocoll. 128 (2022), 107572, https://doi.org/10.1016/j.foodhyd.2022.107572.
[7] K. Torpol, S. Sriwattana, J. Sangsuwan, P. Wiriyacharee, W. Prinyawiwatkul, Optimising chitosan–pectin hydrogel beads containing combined garlic and holy basil essential oils and their application as antimicrobial inhibitor, Int.J.Food Sci. Technol. 54 (6) (2019) 2064–2074, https://doi.org/10.1111/ijfs.14107.
[8] R.-Y. Tsai, P.-W. Chen, T.-Y. Kuo, C.-M. Lin, D.-M. Wang, T.-Y. Hsien, H.-J. Hsieh, Chitosan/pectin/gum arabic polyelectrolyte complex: process-dependent appearance, microstructure analysis and its application, Carbohydr. Polym. 101 (2014) 752–759, https://doi.org/10.1016/j.carbpol.2013.10.008.
[9] V.B.V. Maciel, C.M.P. Yoshida, T.T. Franco, Chitosan/pectin polyelectrolyte complex as a pH indicator, Carbohydr. Polym. 132 (2015) 537–545, https://doi.org/10.1016/j.carbpol.2015.06.047.
[10] X. Niu, A. Liu, C. Liu, C. Zhang, S.S. Low, P.L. Show, Small laccase from Streptomyces coelicolor catalyzed chitosan–pectin blending film for hazardous gas removal, Environ.Technol.Innov. 23 (2021), 101690, https://doi.org/10.1016/j.eti.2021.101690.
[11] N. Chausali, J. Saxena, R. Prasad, Recent trends in nanotechnology applications of bio-based packaging, J.Agric.Food Res. 7 (2022), 100257, https://doi.org/10.1016/j.jafr.2021.100257.
[12] S. Pirsa, I.K. Sani, S.S. Mirtalebi, Nano-biocomposite based color sensors: investigation of structure, function, and applications in intelligent food packaging, Food Packag. Shelf Life 31 (2022), 100789, https://doi.org/10.1016/j.fpsl.2021.100789.
[13] M.V. Nikolic, Z.Z. Vasiljevic, S. Auger, J. Vidic, Metal oxide nanoparticles for safe active and intelligent food packaging, Trends Food Sci. Technol. 116 (2021) 655–668, https://doi.org/10.1016/j.tifs.2021.08.019.
[14] V. Galstyan, M. Bhandari, V. Sberveglieri, G. Sberveglieri, E. Comini, Metal oxide nanostructures in food applications: quality control and packaging, Chemosensors 6 (2) (2018) 16, https://doi.org/10.3390/chemosensors6020016.
[15] M. Appu, Z. Lian, D. Zhao, J. Huang, Biosynthesis of chitosan-coated iron oxide (Fe3O4) hybrid nanocomposites from leaf extracts of Brassica oleracea L. and study on their antibacterial potentials, 3 Biotech 11 (6) (2021) 271, https://doi.org/10.1007/s13205-021-02820-w.
[16] T. Yeamsuksawat, H. Zhao, J. Liang, Characterization and antimicrobial performance of magnetic Fe3O4@chitosan@Ag nanoparticles synthesized via suspension technique, Mater.Today Commun. 28 (2021), 102481, https://doi.org/10.1016/j.mtcomm.2021.102481.
[17] W. Wu, M. Jia, Z. Zhang, X. Chen, Q. Zhang, W. Zhang, P. Li, L. Chen, Sensitive, selective and simultaneous electrochemical detection of multiple heavy metals in environment and food using a lowcost Fe3O4 nanoparticles/fluorinated multi-walled carbon nanotubes sensor, Ecotoxicol. Environ. Saf. 175 (2019) 243–250, https://doi.org/10.1016/j.ecoenv.2019.03.037.
[18] Ayatollah Amoli Branch Department of Food Science and Technology Islamic Azad University, R. Abdi, Determining caffeic acid in food samples using a voltammetric sensor amplified by Fe3O4 nanoparticles and room temperature ionic liquid, Int. J. Electrochem. Sci. (2020) 2539–2548, https://doi.org/10.20964/2020.03.30.
[19] H. Zhang, X. Ma, Y. Liu, N. Duan, S. Wu, Z. Wang, B. Xu, Gold nanoparticles enhanced SERS aptasensor for the simultaneous detection of salmonella typhimurium and Staphylococcus aureus, Biosens. Bioelectron. 74 (2015) 872–877, https://doi.org/10.1016/j.bios.2015.07.033.
[20] D20 Committee, n.d.D20 Committee . (n.d.). Test Method for Tensile Properties of Plastics. ASTM International. doi:10.1520/D0638-14.
[21] I. Zarandona, C. Bengoechea, E. Álvarez-Castillo, K. de la Caba, A. Guerrero, P. Guerrero, 3D printed chitosan-pectin hydrogels: from rheological characterization to scaffold development and assessment, Gels 7 (4) (2021) 175, https://doi.org/10.3390/gels7040175.
[22] N. Li, H. Ke, T. Wang, S. Xia, Recyclable surface-functionalized Fe3O4 particles for heavy oil viscosity reduction, J. Pet. Sci. Eng. 211 (2022), 110112, https://doi.org/10.1016/j.petrol.2022.110112.
[23] S.D. Pasini Cabello, N.A. Ochoa, E.A. Takara, S. Mollá, V. Compañ, Influence of pectin as a green polymer electrolyte on the transport properties of chitosan-pectin membranes, Carbohydr. Polym. 157 (2017) 1759–1768, https://doi.org/10.1016/j.carbpol.2016.11.061.
[24] G.O. Akalin, O. Oztuna Taner, T. Taner, The preparation, characterization and antibacterial properties of chitosan/pectin silver nanoparticle films, Polym. Bull. 79 (6) (2022) 3495–3512, https://doi.org/10.1007/s00289-021-03667-0.
[25] M. Salari, M. Sowti Khiabani, R. Rezaei Mokarram, B. Ghanbarzadeh, H. Samadi Kafil, Development and evaluation of chitosan based active nanocomposite films containing bacterial cellulose nanocrystals and silver nanoparticles, Food Hydrocoll. 84 (2018) 414–423, https://doi.org/10.1016/j.foodhyd.2018.05.037.
[26] S. Venkateswarlu, B. Natesh Kumar, B. Prathima, K. Anitha, N.V.V. Jyothi, A novel green synthesis of Fe3O4-Ag core shell recyclable nanoparticles using Vitis vinifera stem extract and its enhanced antibacterial performance, Phys. B Condens. Matter 457 (2015) 30–35, https://doi.org/10.1016/j.physb.2014.09.007.
[27] A. Reizabal, C.M. Costa, N. Pereira, L. Pérez-Álvarez, J.-L. Vilas-Vilela, S. Lanceros-Méndez, Silk fibroin based magnetic nanocomposites for actuator applications, Adv. Eng. Mater. 22 (6) (2020), 2000111, https://doi.org/10.1002/adem.202000111.
[28] M.J. Kishor Kumar, J.T. Kalathi, Interface dominated dielectric response of PS-Fe 3 O 4 patchy microspheres, Langmuir 35 (43) (2019) 13923–13933, https://doi.org/10.1021/acs.langmuir.9b02117.
[29] A. Radoń, D. Łukowiec, M. Kremzer, J. Mikuła, P. Włodarczyk, Electrical conduction mechanism and dielectric properties of spherical shaped Fe3O4 nanoparticles synthesized by co-precipitation method, Materials 11 (5) (2018) 735, https://doi.org/10.3390/ma11050735.
[30] T. Tuesta-Chavez, J. Monteza, M.I. Silva Jaimes, G.A. Ruiz-Pacco, K. Changanaqui, J.B. Espinoza-Suarez, H. Alarcon, A.M. Osorio-Anaya, A.C. Valderrama-Negrón, M. D.P.T. Sotomayor, Characterization and evaluation of antioxidant and antimicrobial capacity of prepared liquid smoke-loaded chitosan nanoparticles, J. Food Eng. 319 (2022), 110912, https://doi.org/10.1016/j.jfoodeng.2021.110912.
[31] A.M. El-Khawaga, A.A. Farrag, M.A. Elsayed, G.S. El-Sayyad, A.I. El-Batal, Antimicrobial and photocatalytic degradation activities of chitosan-coated magnetite nanocomposite, J. Clust. Sci. 32 (5) (2021) 1107–1119, https://doi.org/10.1007/s10876-020-01869-6.
[32] D.M.S.A. Salem, M.M. Ismail, M.A. Aly-Eldeen, Biogenic synthesis and antimicrobial potency of iron oxide (Fe3O4) nanoparticles using algae harvested from the Mediterranean Sea,Egypt, Egypt. J. Aquat. Res. 45 (3) (2019) 197–204, https://doi.org/10.1016/j.ejar.2019.07.002.